



ELSEVIER

Journal of Nuclear Materials 278 (2000) 11–19

Journal of  
nuclear  
materials

www.elsevier.nl/locate/jnucmat

# Fe–15Ni–13Cr austenitic stainless steels for fission and fusion reactor applications. II. Effects of minor elements on precipitate phase stability during thermal aging

E.H. Lee\*, L.K. Mansur

*Metals and Ceramics Division, Oak Ridge National Laboratory, P.O. Box 2008, Oak Ridge, TN 37831-6376, USA*

Received 3 May 1999; accepted 13 September 1999

## Abstract

The precipitate phase stability in Fe–15Ni–13Cr base austenitic alloys was investigated as a function of minor alloying additions after thermally aging at 600°C and 675°C for times ranging from 24 h to one year. Seven major precipitate phases were found in aged specimens, including  $M_{23}C_6$ , Laves, Eta ( $\eta$ ), TiO, NbC, MC, and  $M_2P$ . The types and amounts of precipitate phases varied with alloying element additions, aging temperature, and aging time. By analyzing the composition of each individual particle, it was possible to determine the essential constituent elements for each phase. From this information, a strategy to promote or suppress certain precipitate phases was developed. Among the seven phases, the most desirable precipitate phases were considered to be MC and  $M_2P$ , because these particles form on a fine scale with a high number density and, therefore, can serve as effective gas atom trap sites under irradiation. © 2000 Elsevier Science B.V. All rights reserved.

PACS: 64.75.+g; 81.30.Mh; 81.40.Cd

## 1. Introduction

Fe–Cr–Ni base austenitic alloys, such as AISI 316 and 304 stainless steels, are used in various industrial applications because they combine outstanding mechanical formability with good higher temperature strength, and oxidation and corrosion resistance. However, it has been found that when these alloys are used under neutron irradiation environment as in nuclear reactor, their serviceable lifetime is greatly compromised due to properties' degradation. The major cause of degradation was attributable to a long term exposure to high energy neutrons and temperature. In the past few decades, considerable progresses have been made in understanding fundamental mechanisms of radiation induced damage and in developing radiation resistant alloys for reactor applications. The most important

agenda was to mitigate the adverse effects caused by transmutation induced helium. Theoretical and experimental work has shown that the most damaging effects at elevated temperature come from agglomeration of helium atoms and vacancies leading to cavity swelling and to grain boundary cavitation and embrittlement [1,2]. Fortunately, however, it was found that such detrimental effects could be suppressed by dispersing helium atoms on precipitate–matrix interfaces. This required high number densities of helium traps, which could be provided by number densities of precipitates. MC carbide and  $M_2P$  phosphide particles were found to be the most effective precipitate phases, because they form in fine scale and in high number density during thermal aging as well as during irradiation [3–5]. However, inducement of such high number density particles requires a fine tuning of alloy composition, which in turn requires understanding of the synergistic effects of alloying elements, thermal aging, and irradiation on phase stability. In Part I (this issue), we present the results of minor alloying element effects on precipitate phases in the melt products and their implications in

\* Corresponding author. Tel.: +1-423 574 5058; fax: +1-423 574 0641.

E-mail address: leeEH@ornl.gov (E.H. Lee).

alloy fabrication. In this paper, we present data on the effects of minor alloying elements on phase stability during thermal aging. In Part III (this issue), we present radiation effects on phase stability under heavy ion irradiation. For neutron irradiation effects, some of the Fast Flux Test Facility (FFTF) reactor data were reported previously [6].

In the past, numerous investigators studied precipitate phases in austenitic steels. Weiss and Stickler documented precipitate phases found in AISI 316 stainless steel [7]. Precipitation reactions in iron-base alloys were reviewed by Decker and Floreen [8] and by Edmond and Honeycombe [9]. However, the information in those reviews was gathered from various sources and the in-

vestigated alloys covered a wide range of base alloy compositions; thus it was difficult to differentiate the effects of minor alloying elements from the effects of base alloy compositions. Moreover, at that time, it was difficult to study the early stages of phase formation because precipitate volume fractions were often too small to be analyzed by conventional bulk analysis methods. However, recent advancements in analytical electron microscopy have made it possible to analyze the micro-chemistry of individual particles and have allowed us to better understand micro-alloying phenomena. In particular, for specimens aged for very short periods of time, the identification and characterization of precipitate phases owe much to carbon-replica extraction and

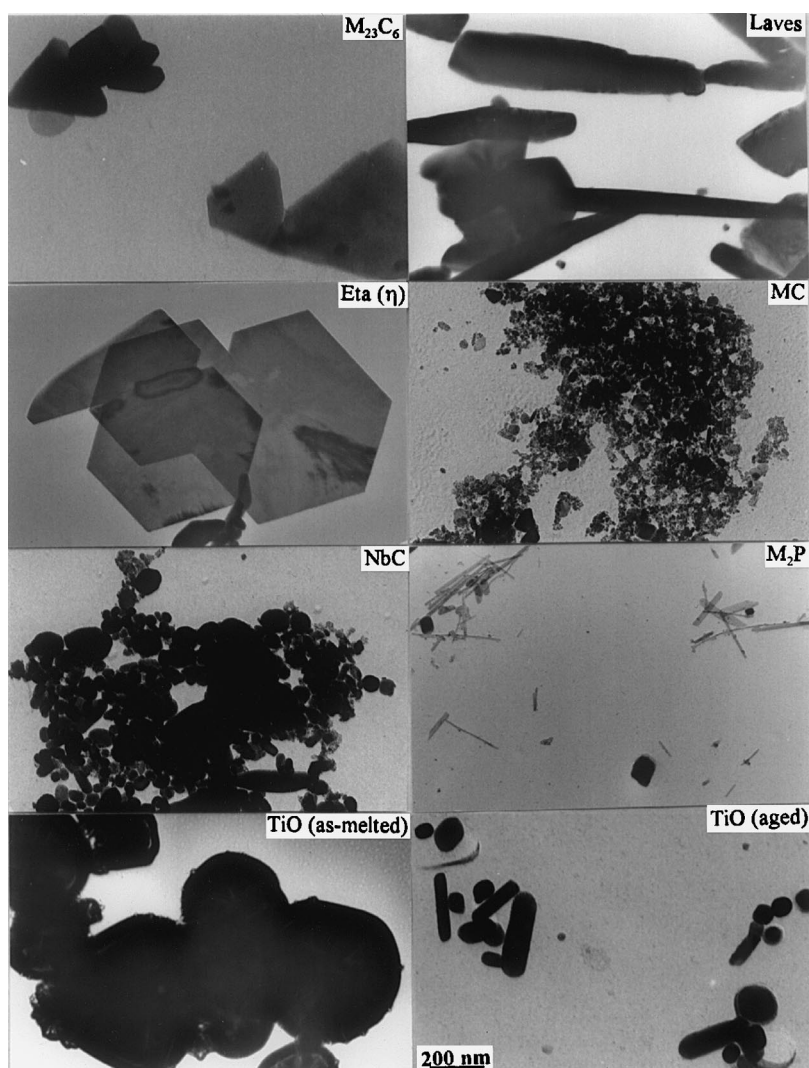


Fig. 1. Typical morphologies of precipitate phases:  $M_{23}C_6$  in B12 (500 h/600°C); Laves in E1 (six months/675°C);  $\eta$  in E4 (six months/675°C); MC in B8 (500 h/675°C); NbC in B13 (500 h/675°C);  $M_2P$  in E9 (six months/675°C); TiO in B2 (as-melted), and TiO in B2 (500 h/600°C).

energy dispersive X-ray spectroscopy techniques. In this work, alloys with various alloying element additions were thermally aged at 600°C and 675°C for various periods of time, and the precipitate phases in the aged specimens were investigated by using transmission electron microscopy (TEM) and energy dispersive X-ray spectroscopy (EDS) methods.

## 2. Experimental

The same 28 Fe–15Ni–13Cr based alloys, whose fabrication was described in Part I, were used to investigate thermal aging effects. As previously described, the alloys were prepared by adding one to several alloying elements to the Fe–15Ni–13Cr ternary alloy.

Typical concentrations of alloying elements were, in weight percent, 2.2 Mn, 2.0 Mo, 0.22 Ti, 0.044 C, 0.85/0.35 Si, 0.05/0.01 P, 0.002 B, and 0.4/0.2 Nb when they were added. Complete alloy compositions can be found in Part I. Here, all alloy compositions are expressed in weight percent (wt%), and precipitate compositions are in atomic percent (at.%). Carbon and oxygen were not included in precipitate compositions due to the limitation of EDS in detecting low mass elements with the instrument used.

Specimens were prepared in the form of TEM disks from 23% cold-worked sheet alloys. Disks were then encapsulated in evacuated and helium back-filled (25 kPa) quartz capsules, and aged at 600°C and 675°C for the periods of 24 h, 500 h, six months, and one year. Crystal structure and microchemical analyses were

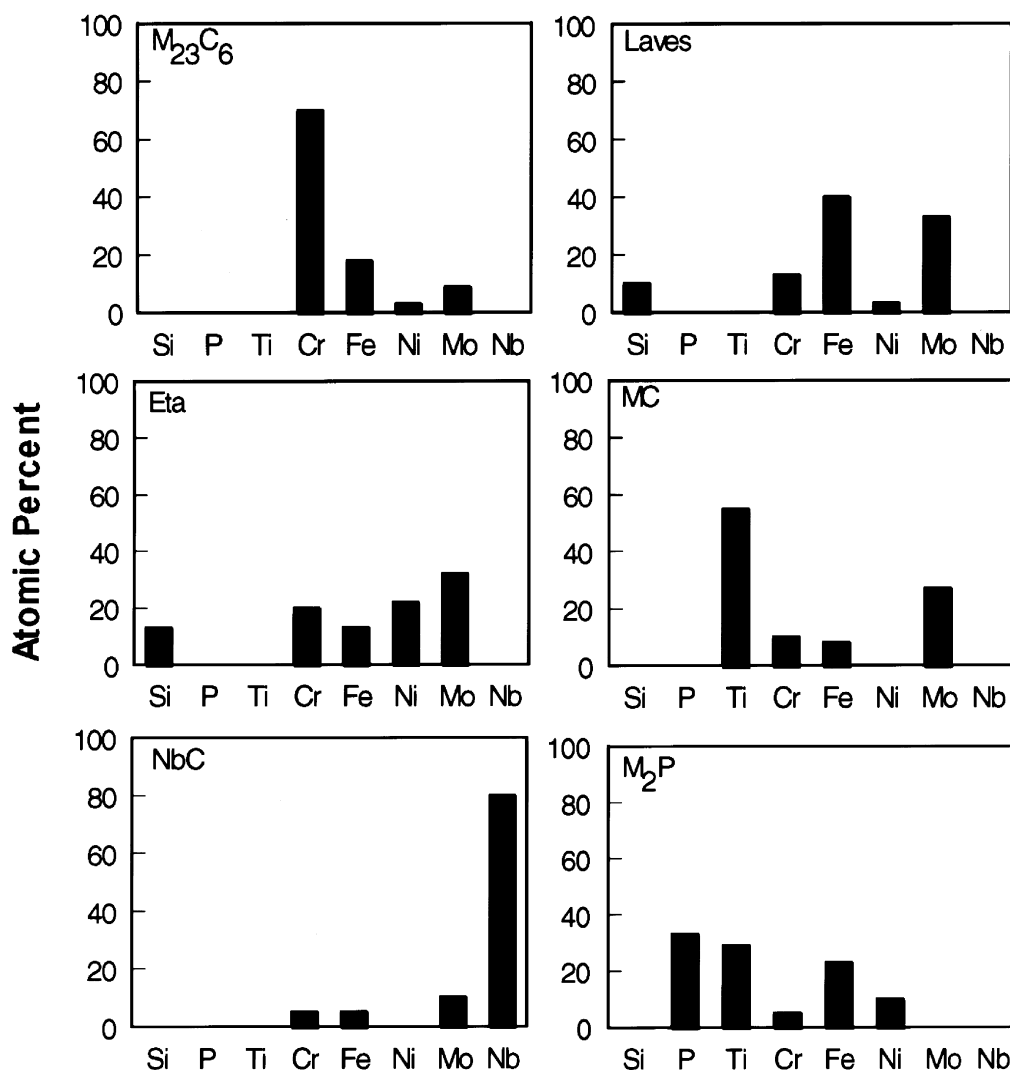


Fig. 2. Typical EDS spectra for the precipitate phases found in Fe–23Cr–15Ni base austenitic steels aged at 600–675°C.

carried out by TEM and EDS for precipitate particles extracted on carbon replicas and also for particles in the thinned TEM foils, following the routine procedures established in previous experiments [10]. Detailed TEM electron diffraction analyses of precipitate phases were also reported in the previous paper and thus are not reiterated here. In general, the morphology and composition of each precipitate phase were so distinct that an experienced microscopist could identify them by their shapes or EDS spectra, even before TEM diffraction analyses. As a guide, typical morphologies of precipitate phases are displayed in Fig. 1 and typical compositional finger prints determined by EDS are illustrated in Fig. 2. For analyses, a JEM-120CX analytical transmission electron microscope equipped with a beryllium window EDS detector was used. In most cases, it was not difficult to distinguish the melt-product precipitate phases from thermal-aging precipitate phases because their particle sizes and morphologies were noticeably different from each other.

### 3. Results

In Part I, we reported 14 precipitate phases which occurred during the alloy melting processes. After thermal aging at 600°C and 675°C, seven major precipitate phases were developed, which included  $M_{23}C_6$ , Laves, Eta ( $\eta$ ), TiO, MC, NbC, and phosphides. Among the seven, the first three were not observed in the melt products, whereas the latter four were observed to a lesser degree after melting but developed significantly more in number but smaller in size during thermal aging. The precipitates in the melt-product were clearly recognized by their large and globular morphology. The precipitates produced by thermal aging were somewhat different in composition (accommodating a wide range of impurity elements), morphology (generally smaller in size and having distinct shapes), abundance (higher in number density), and distribution (more uniform in size and space), even though they had the same crystal

structure as the corresponding melt product phase. Table 1 summarizes the crystallographic information of these precipitate phases. The types of precipitate phases and amounts found varied from alloy to alloy because of the difference in alloy compositions, as summarized in Table 2. Critical changes in alloying additions are indicated next to the alloy symbols, to better illustrate the relationship between alloy composition and the precipitate phases found. When Laves,  $M_{23}C_6$ , and  $\eta$  were present, they were large sized particles that comprised most of the precipitate volume fraction. By comparison, MC,  $M_2P$ , and NbC precipitates were finer, higher number density phases but comprised only a minor volume fraction of the total precipitation.

All seven precipitate phases could be identified after only 24 h of aging, although their volume fractions were extremely small, particularly for the Laves and phosphide phases. Precipitate volume fractions increased with increasing aging time and temperature. Most precipitate phases became quite copious after 500 h of aging. For a given alloy, the precipitate compositions were rather insensitive to aging time and temperature, but same precipitate phase in two different alloys showed somewhat different compositions. In the following, specific characteristics of each precipitate phase are described.

#### 3.1. $M_{23}C_6$

After thermal aging, profuse  $M_{23}C_6$  particles were formed in all carbon containing alloys, mostly at grain boundaries and along deformation bands. A few  $M_{23}C_6$  particles were also found even in alloys with no carbon addition because of the presence of trace impurity carbon (<0.01 wt%). The  $M_{23}C_6$  phase was characterized by a strong Cr-peak in EDS. Although  $M_{23}C_6$  particles accommodated a range of compositions, their constituent elements were strictly limited to Cr, Fe, Ni, and Mo. There were two types of  $M_{23}C_6$  depending upon molybdenum addition, namely  $(Cr, Fe, Ni)_{23}C_6$  and  $(Cr, Fe, Ni, Mo)_{23}C_6$  as summarized in Table 3. When Mo

Table 1  
Crystallographic information of precipitate phases

Phases	Crystal structure/space group	Lattice parameter (nm)	Orientation to matrix	Typical morphology
$M_{23}C_6$	Cubic, D8 <sub>4</sub> , Fm $\bar{3}$ m	$a_0 = 1.06$	Cube-on-cube or twin	Rhombohedral platelet
Laves	Hex., C14, P6 <sub>3</sub> /mmc	$a_0 = 0.41$ $c_0 = 0.77$	Various orientations	Faulted lath
$\eta$	Cubic, E9 <sub>3</sub> , Fd $\bar{3}$ m	$a_0 = 1.08$	Cube-on-cube	Hexagonal
TiO	Cubic, B1, Fm $\bar{3}$ m	$a_0 = 0.43$	Cube-on-cube	Short rod
MC	Cubic, B1, Fm $\bar{3}$ m	$a_0 = 0.432$	Cube-on-cube	Small sphere
NbC	Cubic, B1, Fm $\bar{3}$ m	$a_0 = 0.447$	Cube-on-cube	Small sphere
$M_2P$	Hex., C <sub>22</sub> , P321	$a_0 = 0.604$ $c_0 = 0.36$	( $\bar{1}\bar{2}10$ )/(011) (0001)/(001)	Thin needle lath

Table 2  
Precipitate phases formed during thermal aging at 600°C and 675°C

Alloys (additions) <sup>a</sup>	Precipitate phases	Alloys (additions) <sup>a</sup>	Precipitate phases
B1 (ternary)	No new phase	E1 (all additions)	Laves, MC, M <sub>23</sub> C <sub>6</sub> , η
B2 (Ti)	TiO	E2 (–Mo)	MC, M <sub>23</sub> C <sub>6</sub>
B3 (Si)	No new phase	E3 (–Mn)	Laves, MC, M <sub>23</sub> C <sub>6</sub> , η
B4 (B)	No new phase	E4 (–Ti)	Laves, M <sub>23</sub> C <sub>6</sub> , η
B5 (Ti, C)	MC, M <sub>23</sub> C <sub>6</sub>	E5 (–C)	Laves, TiO
B6 (Ti, C, Mo)	MC, M <sub>23</sub> C <sub>6</sub> , Laves	E6 (0.3Si)	Laves, MC, M <sub>23</sub> C <sub>6</sub>
B7 (Ti, C, Si)	MC, M <sub>23</sub> C <sub>6</sub>	E7 (–Si)	Laves, MC, M <sub>23</sub> C <sub>6</sub>
B8 (Ti, C, B)	MC, M <sub>23</sub> C <sub>6</sub>	E8 (0.8Si, P)	M <sub>2</sub> P, Laves, MC, M <sub>23</sub> C <sub>6</sub> , η
B9 (P)	No new phase	E9 (0.3Si, P)	M <sub>2</sub> P, Laves, MC, M <sub>23</sub> C <sub>6</sub> , η
B10 (P, Si)	M <sub>2</sub> P	E10 (–Si, P)	M <sub>2</sub> P, Laves, MC, M <sub>23</sub> C <sub>6</sub>
B11 (P, Ti, C)	M <sub>2</sub> P, MC, M <sub>23</sub> C <sub>6</sub>	E11 (0.8Si, –Ti, 0.4Nb)	NbC, Laves, M <sub>23</sub> C <sub>6</sub> , η
B12 (P, Ti, C, Si)	M <sub>2</sub> P, MC, M <sub>23</sub> C <sub>6</sub>	E12 (0.3Si, –Ti, 0.4Nb)	NbC, Laves, M <sub>23</sub> C <sub>6</sub>
B13 (Nb, C)	NbC, M <sub>23</sub> C <sub>6</sub>	E13 (–Si, –Ti, 0.4 Nb)	NbC, Laves, M <sub>23</sub> C <sub>6</sub>
B14 (0.01P)	No new phase	E14 (–Si, 0.1Ti, 0.2 Nb)	NbC, Laves, MC, M <sub>23</sub> C <sub>6</sub>

<sup>a</sup> Nominal composition of base ternary B1 alloy is Fe–13Cr–15Ni and that of engineering E1 alloy is Fe–13Cr–15Ni–2Mo–2Mn–0.2Ti–0.04C–0.8Si. Added or omitted elements are indicated in the parentheses. Phosphorous additions are about 0.05 wt% unless specified. A small amount of boron (<0.002 wt%) was added in alloys B4 and B8.

Table 3  
Composition ranges (at.%) for the precipitate phases formed during thermal aging at 600–675°C<sup>a</sup>

Phases	Si	P	Ti	Cr	Fe	Ni	Mo	Nb	Alloying additions
M <sub>23</sub> C <sub>6</sub>	–	–	–	73–82	15–22	2–6	–	–	–Mo
	–	–	–	54–79	12–22	2–11	6–16	–	+Mo
Laves	5–12	–	–	9–19	33–44	3–11	32–37	–	0.8Si
	4–9	–	–	10–14	36–34	6–7	27–39	–	0.3Si
	–	–	–	10–21	37–48	3–8	29–37	–	0.0Si
	0–9	–	–	9–12	36–47	4–9	26–36	2–10	+Nb
η	5–9	–	0–2	19–43	9–16	11–26	23–36	–	+Si + Mo, 600°C
	9–17	–	0–6	12–28	12–17	16–23	32–41	–	+Si + Mo, 675°C
TiO	–	–	100	–	–	–	–	–	–C(B2, E5)
MC	–	–	64–94	0–36	0–2	–	–	–	–Mo
	–	–	29–77	3–20	0–18	–	12–43	–	+Mo
NbC	–	–	–	0–7	0–10	–	9–17	65–83	–Ti
	–	–	7–32	2–16	2–8	–	1–9	62–71	+Ti
	–	–	–	–	–	–	–	100	+C + Nb (B13)
M <sub>2</sub> P	–	30–37	17–37	0–14	20–32	0–12	(9–11) <sup>b</sup>	–	+P + Si/Ti, 675°C
M <sub>3</sub> P	–	22–26	23–50	5–13	14–29	0–16	–	–	+P + Si/Ti, 675°C
M <sub>5–6</sub> P	–	13–18	0–15	22–34	36–43	10–12	–	–	+P + Si/Ti, 600°C

<sup>a</sup> Carbon and oxygen are not counted in composition because of EDS limitation.

<sup>b</sup> For E-series alloys with Mo.

was present, Cr content in the phase decreased. M<sub>23</sub>C<sub>6</sub> phase accommodated the constituent elements in varying ratios and showed no apparent compositional variation with aging time and temperature. When Nb and/or Ti was present, M<sub>23</sub>C<sub>6</sub> was noticeably reduced because carbon was depleted by NbC and/or MC carbide formation. Phosphorous addition promoted M<sub>23</sub>C<sub>6</sub> formation (B10, B11, B12, E9, E10) or η (E8), because titanium was consumed by Ti-rich phosphide, reducing

MC formation, and thus resulting in excess carbon available for M<sub>23</sub>C<sub>6</sub> or η. The enhancement of M<sub>23</sub>C<sub>6</sub> phase was also observed in C + P and C + N + P austenitic steels by Irvine et al. [11], Dulis [12] and Saatinen [13]. They attributed the M<sub>23</sub>C<sub>6</sub> enhancement to the phosphorous entering into the precipitating carbides as M<sub>23</sub>(C, P)<sub>6</sub> [11] or (Cr, Fe, P)<sub>23</sub>C<sub>6</sub> [12,13]. These conclusions were made based on measurements of lattice parameters and *average* compositions of extracted

particles, not on an analysis of individual particles. However, EDS analysis of individual particles clearly revealed that there was no phosphorous in  $M_{23}C_6$  phase, but rather  $M_2P$  and  $M_{23}C_6$  particles coexisted as two distinct phases. Since  $M_{23}C_6$  particles generally constituted most of the precipitate volume fraction because of large sizes, averaging particle composition with larger electron probes in previous work might have sampled mostly  $M_{23}C_6$ , but clearly that is not the case using smaller electron probes with higher spatial resolution in this work.

### 3.2. Laves

Laves phase particles were found in all alloys with Mo additions. Although Laves formation was sluggish compared to other phases, a few Laves particles were observed after 24 h of aging. The Laves nucleation sites were primarily associated with defects such as dislocations, grain boundaries, twin boundaries, and deformation bands. Laves particles could be identified easily by their blocky or elongated lath morphology with internal faulted defect structure. Analyses revealed that Laves phase had about 33 at.% Mo, approximately in  $M_2Mo$  stoichiometric ratio. The two third M sites were occupied mainly by Fe with varying amounts of Cr, Ni, and Si. Although Si was not an essential ingredient for Laves phase, the Si fraction in Laves and the Laves volume fraction increased with increasing Si concentration in alloys. Among 45 spectra recorded, only four showed a small titanium peak, hinting that Ti might not be a Laves ingredient and that the erroneous Ti-peak might have originated from small MC particles attached to Laves during extraction. When Nb was present, Laves formation was enhanced. Analyses of particle compositions revealed  $(Mo + Nb) \approx 33$  at.% suggesting that Nb occupied Mo-sites. Laves was suppressed by MC, because MC phase accommodated Mo as high as 43 at.%. Under conditions more favorable for MC (i.e., high Ti supersaturation and high dislocation density), Laves was further suppressed, suggesting kinetic competition between the two phases. MC nucleates in less than a minute at 600°C.

### 3.3. Eta ( $\eta$ )

$\eta$  phase particles were found only in alloys having C, Si, and Mo together. Crystal structure of  $\eta$  phase was confirmed to be  $Fd\bar{3}m$  diamond cubic by analyzing electron diffraction patterns obtained from the extracted particles.  $\eta$  particles appeared in thin diamond or hexagonal platelet morphology and their detection in TEM was extremely difficult because the thin platelet could not be imaged easily. When either Si or C level was lowered,  $\eta$  was suppressed. Similar to the  $M_{23}C_6$  case, phosphorous promoted  $\eta$  because phosphide accom-

modated Ti, discouraging MC formation and thus leaving more C in solution for  $\eta$  phase. Different from  $M_{23}C_6$  and Laves phases,  $\eta$  composition varied with temperature; the (Si, Mo)/Cr ratio increased when aging temperature increased from 600°C to 675°C. Two types of diamond cubic  $\eta$  phase were reported [14], filled type  $M_6C$  and unfilled type  $M_3SiX$ , with Si being on a metal site and X being a vacant site. Complex carbides derived from the parent lattice  $Ti_2Ni$  ( $\eta$ ) are also called eta carbides which include  $M_3M'_3C$  ( $\eta_1$ ),  $M_2M'_4C$  ( $\eta_2$ ), and  $M_6M'_6C$  ( $\eta_3$ ) types having lattice parameter in the range of  $a_0 = 1.1\text{--}1.2$  nm [15]. However, the present work showed that both C and Si were essential elements for  $\eta$  phase. Thus  $\eta$  phase is believed to be a carbosilicide in the form of  $(M, Si)_6C_x$ , with  $x < 1$ .

### 3.4. MC

MC denotes the fcc TiC phase which accommodates other minor metallic elements. Since there exists impurity nitrogen in all alloys, nitrogen is known to be present in the carbide as  $M(C, N)$ . However, N was not detected in MC phase by electron energy loss spectroscopy (EELS) [4]. As pointed out already, EDS did not include C, O, and N analyses, and thus here we will simply designate the carbide as MC. There were large primary MC particles in all Ti and C containing alloys prior to thermal aging. A very high number density of fine secondary MC particles (20–30 nm) evolved at dislocations during thermal aging. Electron diffraction analyses revealed that the small size MC particles had the characteristic cube-on-cube relation with the austenitic matrix. The major constituents of MC phase were Ti, Mo, and Cr with sporadic inclusions of Fe and Ni. Similar type MC phase was also reported previously [16–18]. Although MC formed without Mo (B5 alloy), MC phase had a strong affinity for Mo and accommodated Mo as high as 43 at.%, such that when MC became dominant, Mo was depleted from solution and Laves was suppressed.

### 3.5. NbC

When Nb and C were present, NbC phase similar to MC was developed at dislocations during thermal aging. Here again NbC may be in the form of  $Nb(C, N)$ , but nitrogen will be ignored in the formula. NbC particles were somewhat coarser and lower in number density compared with MC particles. Differing from the NbC phase (100% Nb in EDS excluding C) found in the melt products, thermal-aging-produced NbC particles (E11, E12, E13) accommodated a wide range of metallic elements, namely in decreasing order, Nb, Mo, Cr, Fe, and infrequently Ni and Mn. Similar NbC particles were also observed in niobium modified austenitic stainless steel previously [17]. When Ti was present (E14), (Nb, Ti)C

phase, with Ti as high as 32 at.%, was developed. When Ti was present, Mo in the phase was reduced as Ti substituted on Nb sites. Although both NbC and MC accommodated Mo, Mo solubility in NbC was less than in MC. On the other hand, Nb was soluble in Laves but Ti was not. For these reasons, Laves was promoted when Nb was present. The Ti/Nb ratios in the (Ti, Nb)C carbide particles were in the range 0.1–0.5. The low Ti level in (Nb, Ti)C phase was believed to be due to low Ti (0.1 wt%) in E14 alloy. Interestingly, NbC particles, in B13 alloy which had only Nb and C additions, did not accommodate any other metallic elements. EDS results showed 100% Nb, again not counting C, O, and/or N. Clearly, further studies are need to understand the synergistic effects of Mo and other alloying elements on the phase stability.

### 3.6. Phosphides

Small globular phosphide particles were found in phosphorous containing alloys prior to thermal aging. After thermal aging, needle-shaped phosphide precipitates were developed at dislocations. The phosphide particles grew with *c*-axis in parallel to the three  $\langle 100 \rangle$  orthogonal directions of the matrix, the direction with the least lattice mismatch. The phosphide structure was confirmed to be hexagonal by analyzing the electron diffraction rings obtained from extracted particles. Phosphide formation was extremely sluggish, almost absent in specimens aged for 24 h, but a scant number of phosphide precipitates was found after 500 h of aging at 600°C and 675°C. Phosphide compositions varied with aging temperature. At 675°C, most phosphide particles had an  $M_2P$  stoichiometric relation, where M represents a mixture of Ti, Fe, Cr, Ni, and Mo in decreasing order when present. A few  $M_3P$  particles were also found. At 600°C, most phosphide particles had initially (500 h) lower phosphorous contents showing  $M_{5-6}P$  stoichiometric relations, but the phosphorous fraction in the phase increased with aging time, resulting in the  $M_2P$  phase after one year of aging. Although phosphide formation was encouraged with increasing Si, interestingly the thermal-aging-produced phosphides did not include Si; phosphides in neutron irradiated stainless steels included up to 16 at.% Si [10]. Titanium being one of the major constituent elements of phosphide, when phosphide became dominant, MC was suppressed as a result of depleted Ti, whereas  $M_{23}C_6$  was encouraged due to conserved C by not forming MC. An excellent review on phosphide phases in binary transition metals was made by Rundquist [19].  $M_2P$  type phosphide was not reported by Rundquist [19], but its presence is indicated in the phase diagram shown in the Binary Alloy Phase Diagrams by Massalski et al. [20]. Profuse needle shaped hexagonal phosphide precipitates were observed in AISI 321 stainless steel held in service at 600°C for 17

yr by Bentley and Leitnaker [21]. The current data, however, suggest that such precipitates might have formed early in the service period. Rowcliffe and Nicholson found  $Cr_3P$  phase in Fe–18Cr–10Ni steel and reported the crystal structure being tetragonal [22]. Although the crystal structure of  $M_3P$  phase could not be determined in this work, we found that phosphide composition changed to become hexagonal  $M_2P$  with increasing aging time.

### 3.7. TiO

Large TiO particles existed in all Ti-containing alloys prior to thermal aging. Nevertheless, additional smaller size TiO particles were formed during thermal aging, but *only* in alloys B2 and E5, which lacked carbon. This finding suggests that some oxygen might have been in solution instead of in oxide form. When sufficient carbon was present, profuse TiC particles formed instead. Although EDS analyses showed 100% Ti (not counting O, C, and/or N) for both melt product TiO and thermal-aging-produced TiO particles, the latter had various distinctive morphologies such as rod, diamond, sphere etc., and could easily be distinguished from the conspicuously large spherical shape melt product TiO particles as shown at the bottom of Fig. 1. Although TiO, TiN, and TiC all have the same  $Fm\bar{3}m$  space group cubic crystal structure and similar lattice parameters, these distinct particles thought to be TiO, since the particles appeared only in B2 and E5 alloys with no carbon addition.

## 4. Discussion

Seven major precipitate phases were identified in Fe–13Cr–15Ni based alloys after thermal aging at 600°C and 675°C. Among the seven, four were carbides,  $M_{23}C_6$ ,  $\eta$ , MC, and NbC, and the other three were Laves, TiO, and phosphides. Laves phase was the unique intermetallic phase found after thermal aging. Although Sigma ( $\sigma$ ) and Chi ( $\chi$ ) phases were often observed in AISI 316 type stainless steels [10], they were not observed in these alloys. Williams investigated precipitate phases in thermally aged austenitic steels [23]. He also found neither  $\sigma$  nor  $\chi$  below 700°C, but observed  $\sigma$  phase in specimens aged between 700°C and 750°C.

Experimental data showed that virtually all alloying elements were found to participate in the precipitate formation as shown in Table 3. One notable observation was that there were no ideal stoichiometric compounds. The X-ray microchemical analyses revealed that the precipitate phases accommodated a wide variety of atomic species in varying proportions, although each phase had characteristic fingerprints in morphology and

composition as shown in Figs. 1 and 2, respectively. The alloying additions did not produce any new phases that have not been observed in AISI 316 type stainless steels. However, types of precipitate phases and their abundance varied considerably depending upon alloying additions. In this experiment, substantial information was gathered to clarify the roles of each alloying element on phase stability. Table 4 summarizes all experimental findings.

Mo was a promoting or stabilizing agent for  $M_{23}C_6$ , Laves, and  $\eta$  phase formation, Nb for NbC, Ti for MC, and P for  $M_2P$ . Among the seven phases,  $M_{23}C_6$ , Laves, and  $\eta$  are considered to be undesirable because they occur in large size and in low number density. In such a case, both gas atoms and vacancies are shared by a small number of precipitates, which results in earlier formation of critical cavity size. Moreover, vacancies are collected more efficiently at large particle interfaces (i.e., point-defect collector effect) [24–26], thereby augmenting void swelling. Besides, Laves phase is considered to have little benefit because large particles contribute very little in strengthening mechanical properties.

TiO formation was triggered mainly by the presence of impurity oxygen and would produce no significant impact in suppressing swelling. Since both NbC and MC phases had a similar crystal structure, (Nb, Ti)C type carbides were formed when both Nb and Ti were present. Gas atom trapping efficiency of NbC phase is smaller than that of MC, because NbC particles are generally larger in size but lower in number density compared with those of MC. Therefore, NbC is considered to be a less desirable phase than MC.

Although Si was not an essential element for  $M_2P$  phase, it promoted  $M_2P$  formation when E8, E9, and

E10 alloys were compared (Table 2). Undesirably, Si also promoted Laves and  $\eta$ . Clearly, an optimal level of Si should be determined to minimize formation of such phases.

Among the seven phases,  $M_2P$  and MC were considered to be the most desirable phases because they nucleate in fine scale and in high number density. Fortunately, in view of designing radiation resistant alloys, the occurrence of  $M_2P$  phase was not affected by other phases because the major constituents of  $M_2P$  phase were Fe and P and no other phases required phosphorous as their constituent. Unfortunately, however, MC was somewhat reduced as a result of dominant Laves phase formation in most alloys investigated in this work, particularly in alloys with phosphorous. Nevertheless, as pointed out in Part I, a considerable fraction of the added Ti was depleted from the matrix by TiO formation with impurity oxygen during alloy melting. Therefore, the suppressed MC could be attributable partly to the lower effective Ti and C concentrations in the alloys investigated here. Phosphorous also tended to promote Laves, because Ti-rich  $M_2P$  depleted Ti, discouraging Mo-rich MC formation. This, however, raises a question whether a microstructure with suppressed Laves phase could be achieved. Incidentally, such example was found in Ti-modified D9 alloy irradiated with neutron at 593°C in the Experimental Breeder Reactor (EBR-II). Laves was suppressed drastically, to the benefit of MC, when Ti supersaturation was increased by dissolving preexisting coarse MC particles back into solution by employing higher solution annealing temperature, 1200°C instead of 1100°C [26].

Mo is known as a solution hardening element and also is important for recrystallization and creep resis-

Table 4  
Role of minor alloying elements on precipitate phases during thermal aging

Precipitate phase	Promoted by	Remarks	Suppressed by	Remarks
$M_{23}C_6$	C P (indirect)	$M_2P$ depletes Ti and avails C for $M_{23}C_6$	Ti, Nb	MC depletes C Essential for $M_{23}C_6$
Laves	Mo, Nb, Si	Constituent elements	C, Ti	MC depletes Mo Essential for Laves
$\eta$ ( $M_6C$ )	Mo, Si, C P (indirect)	$M_2P$ depletes Ti and avails C for $M_6C$	Ti, Nb	MC depletes C Essential for $M_6C$
TiO	Ti	Residual oxygen No significance	C	C promotes MC
MC <sup>a</sup>	Ti, C, (Mo)	Constituent elements	Nb	Nb promotes Laves and depletes Mo needed for MC
NbC	Nb, C	Constituent elements	Ti	Ti competes with Nb
$M_2P$ <sup>b</sup>	P, Fe	Constituent elements	No apparent suppressor	But require enough P to produce high number density $M_2P$

<sup>a</sup> MC particles nucleate in high number density very rapidly (<1 min) at dislocations and exhaust nucleation sites, and thus the formation of sluggish large precipitate phases such as Laves,  $M_{23}C_6$ , and  $\eta$  is suppressed when MC becomes dominant.

<sup>b</sup>  $M_2P$  phase accommodates Ti but not C, so if there is not enough Ti, MC phase may be suppressed whereas  $M_{23}C_6$  is promoted. An optimum balance of Ti, C, and P is required to achieve a high number density of both MC and  $M_2P$  particles.

tance [27]. Although Mo is a common ingredient for Laves,  $M_{23}C_6$ , and  $\eta$ , careful examination of experimental data suggests that Mo reduction may not be necessary if MC and  $M_2P$  were maximized by optimizing P, Ti, and C concentrations. It was reported that MC and  $M_2P$  improved hardness, yield strength, tensile strength, and creep properties due to dislocation pinning by high number density small particles [12,23,28]. Enhancement of MC and  $M_2P$  by optimizing alloy composition is desirable.

## 5. Conclusions

Effects of alloying elements on precipitate phase stability were investigated for Fe–13Cr–15Ni based alloys aged at 600°C and 675°C for periods from 24 h to one year. Seven major precipitate phases,  $M_{23}C_6$ , Laves, Eta ( $\eta$ ), TiO, NbC, MC, and  $M_2P$ , were evolved during thermal aging. It was found that the stability of precipitate phases depend strongly upon alloy composition and thermo-mechanical treatment (i.e., high temperature solution annealing and cold working). Therefore, alloys with desired precipitate phases could be tailored by optimizing alloying element additions—enhancement of MC and/or  $M_2P$  phases by controlling Ti, P, and C levels for example. This, however, requires a detailed knowledge of how minor alloying elements affect the phase stability and what is the impact of thermal aging on precipitate phases. This work establishes a basis to answer these questions and provides guidance in alloy design. The most important and pertinent experimental findings are summarized in Table 4.

Finally, MC and  $M_2P$  strengthened alloys are known to have also excellent thermo-mechanical properties [28], and the efforts to develop radiation resistant alloys benefit not only reactor materials applications but also other critical materials applications, such as high temperature service.

## Acknowledgements

This research was sponsored by the Division of Materials Sciences, US Department of Energy, under contract No. DE-AC05-96OR22464 with Lockheed Martin Energy Research Corporation. The authors wish to thank Drs P.J. Maziasz and S. Babu for reviewing the manuscript.

## References

[1] L.K. Mansur, in: Gordon R. Freeman (Ed.), Kinetics of Nonhomogeneous Processes, ch. 8, Wiley, New York, 1987, p. 377.

- [2] E.H. Lee, L.K. Mansur, Metall. Trans. 21A (1990) 1021.  
 [3] W. Kesternich, J. Nucl. Mater. 127 (1983) 153.  
 [4] P.J. Maziasz, R.L. Klueh, R.F. Rowcliffe, MRS Bull. 14 (1989) 36.  
 [5] E.H. Lee, L.K. Mansur, Philos. Mag. A 61 (1990) 733.  
 [6] E.H. Lee, N.H. Packan, in: N.H. Packan, R.E. Stoller, A.S. Kumar (Eds.), Effects of Radiation on Materials: 14th International symposium, ASTM STP 1046, vol. 1, American Society for Testing and Materials, Philadelphia, 1989, p. 133.  
 [7] B. Weiss, R. Stickler, Metall. Trans. 3 (1972) 181.  
 [8] R.F. Decker, S. Floreen, in: K.C. Russell, H.I. Aaronson (Eds.), Precipitation Process in Solids, TMS-AIME, 1976, p. 63.  
 [9] D.V. Edmonds, R.W.K. Honeycombe, in: K.C. Russell, H.I. Aaronson (Eds.), Precipitation Process in Solids, TMS-AIME, 1976, p. 121.  
 [10] E.H. Lee, P.J. Maziasz, R.F. Rowcliffe, in: J.R. Holland, L.K. Mansur, D.I. Potter (Eds.), Phase Stability During Irradiation, AIME, 1981, p. 191.  
 [11] J.K. Irvine, D.T. Llewellyn, F.B. Pickering, J. Iron Steel Inst. 199 (1961) 153.  
 [12] E.J. Dulis, Iron and Steel Inst. Special Report No. 86 (1964) 162.  
 [13] A.V.A. Saatinen, Scand. J. Met. 2 (1973) 161.  
 [14] H.H. Stadelmaier, Metal Rich Metal–Metalloid Phases, Developments in the Structural Chemistry of Alloy Phases, Plenum, New York, 1969.  
 [15] H. Nowotony, P. Ettmayer, J. Inst. Met. 97 (1969) 180.  
 [16] E.H. Lee, N.H. Packan, L.K. Mansur, J. Nucl. Mater. 117 (1983) 123.  
 [17] P.J. Maziasz, in: J.R. Holland, L.K. Mansur, D.I. Potter (Eds.), Phase Stability During Irradiation, AIME, 1981, p. 477.  
 [18] H.O. Andren, A. Henjered, H. Norden, J. Mater. Sci. 15 (1980) 2365.  
 [19] Stig Rundquist, Ark. Kemi 20 (1962) 67.  
 [20] T.B. Massalski et al. (Eds.), Binary Alloy Phase Diagrams, American Society for Metals, Metals Park, OH, 1986.  
 [21] J. Bentley, J.M. Leitnaker, in: E.W. Collings, H.W. King (Eds.), The Metal Science of Stainless Steels, Met. Soc. AIME, 1978, p. 70.  
 [22] A.F. Rowcliffe, R.B. Nicholson, Acta Metall. 20 (1972) 143.  
 [23] T.M. Williams, in: H.R. Brager, J.S. Perrin (Eds.), Effects of Radiation on Materials, ASTM STP 782, 1982, p. 166.  
 [24] L.K. Mansur, Philos. Mag. 44 (1981) 867.  
 [25] E.H. Lee, A.F. Rowcliffe, L.K. Mansur, J. Nucl. Mater. 103, 104 (1981) 1475.  
 [26] E.H. Lee, L.K. Mansur, Metall. Trans. 23A (1992) 1977.  
 [27] R.W.K. Honeycombe, Steels-Microstructure and Properties, American Society for Metals, Edward Arnold, Great Britain, 1981.  
 [28] P.J. Maziasz, R.W. Swindeman, The International Conference on Advances in Material Technology for Fossil Power Plants, ASM International, Chicago Il., 1–3 September 1987, 8706-018.